Chemical Science

ROYAL SOCIETY OF CHEMISTRY

EDGE ARTICLE

View Article Online
View Journal | View Issue

Cite this: *Chem. Sci.*, 2021, **12**, 12400

All publication charges for this article have been paid for by the Royal Society of Chemistry

Received 18th June 2021
Accepted 12th August 2021

DOI: 10.1039/d1sc03310g

rsc.li/chemical-science

Imaging the oxygen wave with a single bioluminescent bacterium†

Yaohua Li,[a] Sa Wang,[a] Xinyu He,[a] Shijun Li,[b] Tianhua Zheng,[c] You-Peng Chen, *[b] Hua Cui *[c] and Wei Wang *[a]

We developed a capability of a monolayer of bioluminescent (BL) bacteria for spatiotemporally visualizing the heterogeneous distribution and dynamic evolution of interfacial oxygen concentration, resulting in the discovery of spontaneous and stochastic oxygen waves at the interface between the substrate and an undisturbed, apparently still solution. Wild type bacteria, *P. phosphoreum*, spontaneously emit light during the native metabolism processes, *i.e.*, bioluminescence. The emission intensity is sensitively regulated by oxygen concentration. By taking the electrolysis of water as a model, it was demonstrated that time-lapsed BL imaging of a bacterial monolayer allowed for visualizing the dynamic distribution of oxygen. The results were quantitatively understood with a physical model involving the diffusion equation and Michaelis–Menten equation. Unexpectedly, further study uncovered a spontaneous and stochastic oxygen wave in a standard well of a microtiter plate, which was subsequently attributed to the inevitable micro-convections induced by inhomogeneous evaporation and thermal fluctuation. Because of the wide application of microtiter plates, this study sheds new light to better understand the apparent heterogeneity in cell-culture and bio-assays.

Introduction

Oxygen is an essential substance to support aerobic respiration and related physiological functions for cells and a significant portion of bacteria.[1] Given the essential roles of oxygen in life processes, numerous efforts have been made to determine the average concentration of oxygen in bulk samples such as solution and atmosphere. They utilize versatile signal transduction mechanisms (titration,[2] electrochemical,[3–5] optical,[6–8] *etc.*) to report the oxygen concentration quantitatively. Although powerful, these single-point devices (oxygen sensors) reported the average concentration of oxygen molecules and lacked spatial resolution. Meanwhile, different types of oxygen-sensitive optical probes have been proposed to image the distribution of oxygen within cells,[9–11] tissues[12,13] and even living beings.[14–16] For example, transition metal complex compounds have been popular choices for oxygen imaging by monitoring the reduced phosphorescence intensity and lifetime in the presence of oxygen due to the oxygen triplet state quenching.[17,18] Hypoxia-sensing fluorescent probes, whose fluorescence is turned on by bio-reductive reaction in hypoxic cells or tissues, are often based on the irreversible process and depend on reductases activity.[19–21] Chromogenic indicators are another option in which the absorption (*i.e.*, color) is changed in the presence of oxygen. Because it involves chemical reactions, this strategy often suffers from slow reaction kinetics and the lack of reversibility.[22]

Bioluminescent (BL) bacteria are living micro-organisms that spontaneously emit light during their metabolism processes. These bacteria endogenously express luciferase to catalyze the reaction between oxygen and certain substrate compounds to generate product molecules in the excited state.[23] Subsequent radiative decay to the ground state results in the emission of light with a characteristic wavelength depending on the type of bacteria. BL has been considered as one of the most sensitive techniques because it does not require excitation light and thus reduces the optical background as much as possible in both detection and imaging applications.[24–26] For example, when expressing the luciferase system in *E. coli*[27] and mammalian cells,[28] these previously dark species were able to emit light as a result of BL processes. In a recent study, BL intensity was used to report the metabolic dynamics of individual spores during sporulation and germination processes. The spores were engineered to express bacterial luciferase upon germination.[29] Such capability makes luciferase a promising alternative to

[a]State Key Laboratory of Analytical Chemistry for Life Science, School of Chemistry and Chemical Engineering, ChemBIC (Chemistry and Biomedicine Innovation Center), Nanjing University, 210023 Nanjing, Jiangsu, China. E-mail: wei.wang@nju.edu.cn

[b]Key Laboratory of the Three Gorges Reservoir Region's Eco-Environment of Ministry of Education, Chongqing University, 400045 Chongqing, China. E-mail: ypchen@cqu.edu.cn

[c]CAS Key Laboratory of Soft Matter Chemistry, iChEM (Collaborative Innovation Center of Chemistry for Energy Materials), Department of Chemistry, University of Science and Technology of China, 230026 Hefei, Anhui, China. E-mail: hcui@ustc.edu.cn

† Electronic supplementary information (ESI) available. See DOI: 10.1039/d1sc03310g

fluorescent proteins for acting as reporters of gene expression and protein function. While different bacteria species rely on different organic substrates, oxygen is required in nearly all the BL bacteria. Early studies have shown that BL bacteria can be used to determine the sub-μM oxygen concentration, owing to the very low enzymatic reaction constant.[30,31] In addition, because the light emission intensity of BL bacteria is also an indicator of the metabolic activity, they have been routinely used in cytotoxicity assays for decades.[32,33] The addition of polluted water into a suspension of BL bacteria immediately decreased the emission intensity. This change can be captured by a portable photo-detector or the naked eye, very suitable for rapid field pollution assessment in emergency events.[34–36] Although powerful, these studies relied on the overall light emission intensity from a bulk suspension of BL bacteria, and lacked sufficient spatial resolution to image and to monitor the spatial distribution as well as dynamic evolution of oxygen.

In this study, we demonstrate the capability of BL imaging of a monolayer of wild type bacteria, *P. phosphoreum*, for real-time mapping the dynamic and heterogeneous distribution of oxygen molecules at the interface in a standard well of a microtiter plate, leading to the discovery of stochastic and dynamic oxygen waves (nonlinear oxygen pattern) for the first time. We developed a surface functionalization method to immobilize BL bacteria on glass coverslips to form a sub-monolayer. Without the need for any excitation light, a camera was used to capture the spontaneous BL emission from the bacterial monolayer with a suitable microscope objective. In order to demonstrate the superior spatial and temporal resolutions of the BL bacteria layer to report the distribution of oxygen molecules, an artificial oxygen wave was firstly created by applying an oxidative potential to a part of the interface to produce an intensive amount of oxygen molecules *via* water electrolysis. The entire generation and diffusion process of the oxygen molecules was clearly monitored by recording the time-lapsed BL images of the bacterial monolayer. The spatial and temporal features of BL images were quantitatively explained by a theoretical model according to the diffusion equation and Michaelis–Menten equation. Finally, when recording a series of time-lapsed BL images of a resting solution, a stochastic and dynamic oxygen wave was observed without disturbing the solution, uncovering a heterogeneous and dynamic distribution of oxygen molecules even in a resting and apparently still solution.

Results and discussion

Dependence of BL intensity on oxygen

We first demonstrate that the BL intensity of *P. phosphoreum* bacteria is sensitively and reversibly regulated by the concentration of oxygen. *P. phosphoreum* is one kind of facultative anaerobic bacteria that endogenously expresses luciferase and catalyzes the oxidation of fatty aldehyde (RCHO) and the reduced flavin mononucleotide ($FMNH_2$), as described in eqn (1). The detailed mechanism involves two steps.[37] First, $FMNH_2$ binds to oxygen to form the peroxyflavin intermediate. Then, this intermediate reacts with aldehyde luciferin to form the flavin peroxyhemiacetal intermediate that decomposes to produce RCOOH and the excited state FMN*. The radiative decay of FMN* to the ground state is accompanied by the emission of light (~490 nm).

$$FMNH_2 + RCHO + O_2 \xrightarrow{\text{luciferase}} FMN + RCOOH + H_2O + h\nu. \quad (1)$$

As can be seen from eqn (1), the BL intensity directly indicated the enzymatic reaction rate, which is sensitively regulated by the concentration of oxygen. This point was validated by two experiments herein. In the first experiment, after rigorously vortexing a suspension of bacteria to enable the efficient and homogeneous supply of oxygen, bright and uniform light emission was observed from the tube, as shown in Fig. 1a(I). After several seconds of resting, only a small portion of the bacteria at the air–liquid interface remained bright (Fig. 1a(II)), because the interface still enabled an efficient supply of oxygen from the atmosphere, while the oxygen molecules inside the bulk suspension were nearly exhausted as a result of aerobic respiration. When the tube was shaken again to re-supply oxygen, uniform BL emission from the entire suspension with similar brightness appeared again (Fig. 1a(III)). This process was repeated three times and the BL intensity curve is shown in Fig. 1b. A video is provided in the ESI (Movie S1†) to display the processes. Note that the bacteria concentration (number density) was rather high in this demo experiment for the ease of naked-eye observations. Therefore, it took only several seconds to exhaust the oxygen within the bulk suspension.

We designed another experiment to further support the dependence of BL intensity on oxygen concentration. After a classical culture on an agarose plate, separated colonies with representative blue-green emission can be easily observed with the naked eye in a dark room (Fig. 1c). When blowing nitrogen gas on the surface of the agarose plate and monitoring the time-

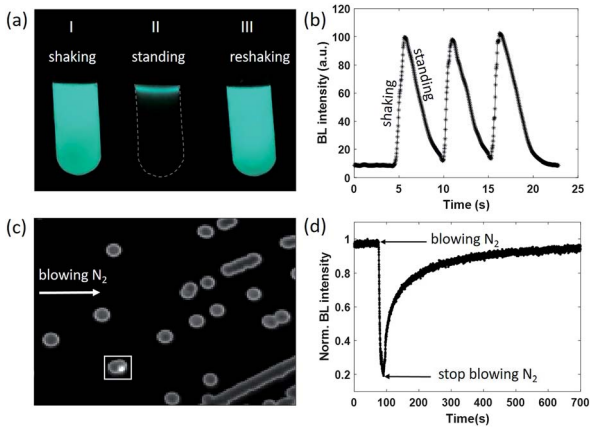

Fig. 1 (a) Representative BL snapshots and (b) the corresponding BL intensity curve during shaking–standing–reshaking of a suspension of BL bacteria. (c) Typical BL image of bacterial colonies cultured in the agarose plate. (d) BL intensity of a colony selected in the white box rapidly decreased when blowing nitrogen, and gradually recovered when re-supplying air.

lapsed BL images, it was found that the BL intensity of the colony marked with the white box significantly decreased by 80% within 20 seconds (Fig. 1d and Movie S2†). Stopping the nitrogen flow resulted in the gradual recovery of BL intensity in another 600 seconds. The slow recovery was due to the limited diffusion of oxygen within the dense colony (~1 mm diameter). Because the bacteria colony itself significantly consumed oxygen during the gas exchange processes, it took a longer time for oxygen to completely recover the bioluminescence intensity. These results clearly indicated that the BL emission was regulated by the oxygen concentration in rapid and reversible manners.

BL imaging of the diffusion of oxygen produced by electrolysis

We next designed an artificially triggered oxygen wave to demonstrate the capability of BL imaging for visualizing the dynamic diffusion of oxygen molecules. A PDMS (polydimethylsiloxane) chamber was placed on a glass coverslip to fabricate a container for bacteria immobilization and BL imaging. The chamber has a diameter of 5 mm, and a height of 8 mm, with a maximum volume of 280 μL, which is the same as a well in a standard 96-well plate. 100 μL of BL bacterial suspension ($OD_{600\ nm} = 1.5$) was dropped into the chamber and we waited for 30 minutes to enable the formation of a monolayer of bacteria on the surface of the coverslip. The coverslip was pre-functionalized with poly-D-lysine to enhance the adhesion due to the electrostatic interaction.[38] After the formation of the monolayer, the suspending bacteria in the solution were removed by gently rinsing the chamber with a clean culture medium several times. The chamber was then filled with 200 μL of culture medium for BL imaging experiments. The formation of a monolayer of BL bacteria was validated by the correlative bright-field (BF) and BL images as shown in Fig. 2a and b, respectively. All the individual bacteria exhibited sufficient light emission, indicating the effective adhesion and good activity of bacterial luciferase.

The coverslip underneath the bacterial monolayer was specially fabricated so that the left half of the coverslip was covered by a 30 nm-thick semi-transparent and conductive platinum (Pt) layer to enable oxygen generation through the electrolysis of water, while the right half was original glass. By introducing counter and reference electrodes into the solution and applying an appropriate potential of 1.5 V to the Pt layer, rapid electrochemical oxidation of water occurred on the Pt side to immediately generate 3.0×10^{-9} mol oxygen molecules in the first second, which subsequently crossed the borderline and diffused towards the right side. The dynamic generation and diffusion of oxygen molecules were visualized by monitoring the time-lapsed BL images as shown in Fig. 2c–f.

Before the electrolysis, BL emission was observed from both sides (Fig. 2c). The Pt side was slightly darker because of the relatively lower transparency, allowing for identifying the borderline as indicated by the white dashed line. At the 20th second, +1.5 V potential was applied to the Pt layer, accompanied by the immediate increase of BL intensity on the left side (Fig. 2d) because of the significantly increased concentration of oxygen and thus the enhanced BL reaction rate. Other potentials have been applied to the Pt layer (Fig. S1†), such as 0.5 V and 1.0 V. The potential of 1.5 V was chosen because of the sufficient signal intensity for quantitative analysis. A narrow BL emission band

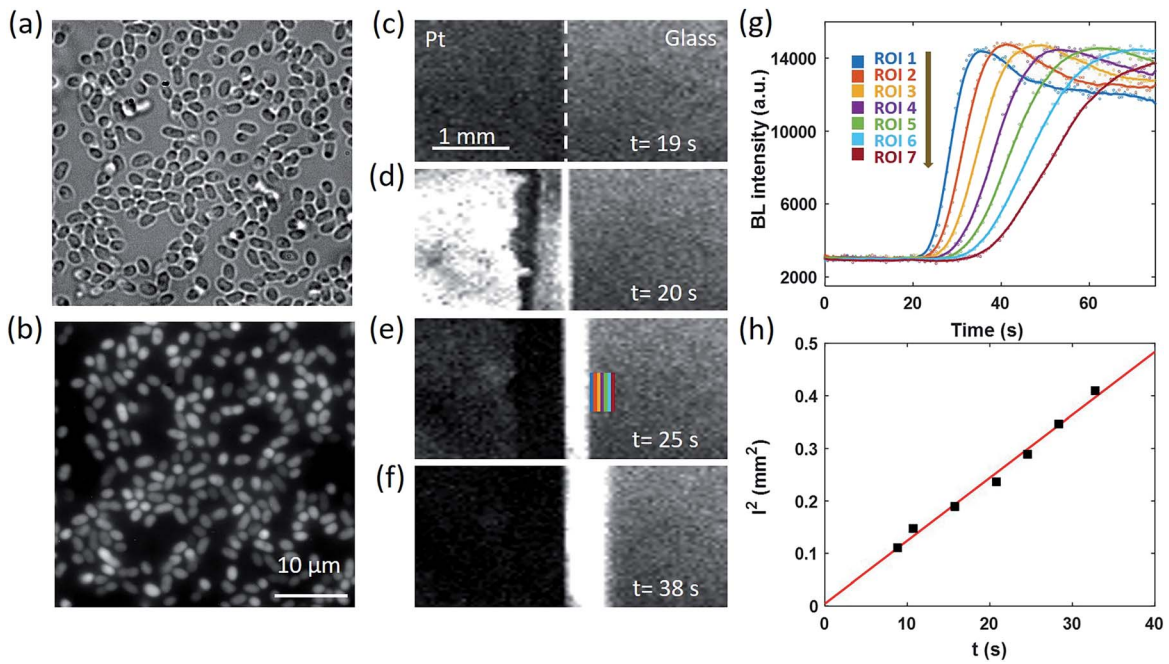

Fig. 2 Correlative BF (a) and BL (b) images of individual BL bacteria. (c)–(f) Time-lapsed BL images reveal the generation and diffusion of oxygen waves in an artificially triggered water electrolysis process (exposure time: 0.63 s.) (g) BL intensity curves of seven ROIs as indicated in (e). (h) Linear dependence of the square of the distance between each ROI and the boundary (l^2) with the time required to reach half-maximal intensity (t).

was also observed penetrating into the glass side by 100 μm, indicating the diffusion of oxygen from the Pt side. In the subsequent several seconds, the BL emission on the Pt side rapidly decreased to nearly zero, which was attributed to the death of bacteria induced by the electroporation and the electrochemical oxidation of important biomolecules under such a high potential. This point was supported by the fact that another electrochemical pulse was not able to recover the BL emission from the Pt side any longer. At the same time, the BL emission band on the glass side continuously expanded towards the right side, which appeared like a migrating BL wave (Fig. 2d–f, and Movie S3†). When selecting seven adjacent regions of interest (ROIs) on the glass side (color rectangles in Fig. 2e) and plotting the local intensity as a function of time, the migration feature is clearly demonstrated in Fig. 2g. At each ROI, the diffusion of oxygen increased the BL emission by roughly four fold to reach a plateau at ~14 000, resulting in an interesting sigmoidal curve. As shown in Fig. 2h, further analysis indicated that there was a linear dependence of the square of the distance between each ROI and the borderline (l^2) with the time required to reach half-maximal intensity (t). According to the three-dimensional diffusion model ($l^2 = 6Dt$),[39] the diffusion coefficient (D) was determined to be $\sim 2.0 \times 10^{-9}$ m^2 s^{-1}, which was consistent with the literature reports.[40,41] It is clear now that the time-lapsed BL images of a bacterial monolayer provide an efficient way to visualize the dynamic distribution of oxygen.

Note that autoinducers were known to enhance the bacteria bioluminescence through the quorum sensing mechanism.[42,43] However, because this mechanism involved the regulation and expression of proteins, it took effect in a typical time scale of tens of minutes (Fig. S2†). Therefore, autoinducers should not interfere with the detection of oxygen in this experiment.

A similar diffusion feature was also validated at a single bacterium level by using a 100× objective to zoom in an 80 × 80 μm^2 region (Fig. 3a). We repeated the electrolysis experiment under 100× magnification with the same experimental conditions and recorded the BL intensity of each single bacterium as a function of time with a temporal resolution of 1 second. A movie consisting of the time-lapsed BL images is provided in Movie S4.† Three representative curves of three individuals (marked by color squares in Fig. 3a) are displayed in Fig. 3b. Similar sigmoidal curves were also observed at a single bacterium level, confirming that the increased BL intensity indeed came from the enhanced enzymatic reaction at higher oxygen concentration. The time required to reach half-maximal BL intensity (t_0) is displayed for each individual bacterium in Fig. 3c. A positive relationship between the position of individual bacteria (x) and t_0 is plotted in Fig. 3d. It further indicated that, as expected, it took a longer time for the oxygen molecules to reach the individual with farther distance.

Physical model

We next built a physical model to explain the sigmoidal curve by using the diffusion equation and Michaelis–Menten equation. When assuming a source with constant oxygen concentration, C_0, to supply oxygen to the surrounding environment *via* diffusion, the centration of local oxygen, $C(r, t)$, as a function of distance (r) and time (t), can be described by the following diffusion equation:[44]

$$C(r,t) = C_0\left[1 - \mathrm{erf}\left(\frac{r}{2\sqrt{Dt}}\right)\right] \quad (2)$$

By assuming a diffusion coefficient of 2.0×10^{-9} m^2 s^{-1}, the relative concentration distribution $C(r, t)$ in a range of 0–1.2 mm within a time window of 40 seconds is shown in Fig. 4a. On the other hand, the dependence of BL intensity with oxygen concentration is described by the Michaelis–Menten equation (eqn (3)). It

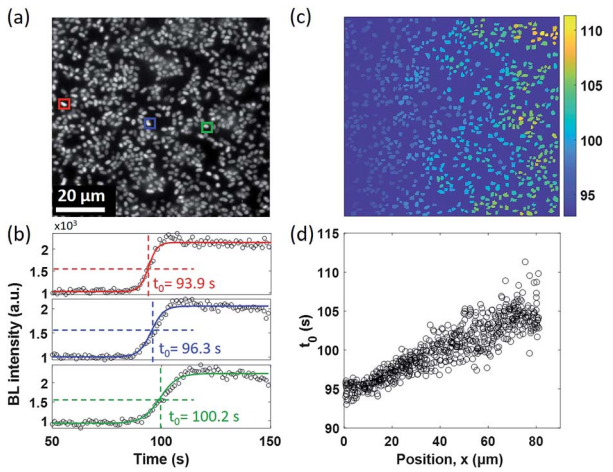

Fig. 3 (a) BL image of a surface-adhered single bacterium. (Exposure time: 1 s.) (b) Representative BL intensity curves of three individuals marked by color squares in (a). (c) The t_0 map of 648 individual bacteria. (d) It demonstrates that it takes a longer time for oxygen to reach the bacteria on the right side, which is consistent with the direction of diffusion.

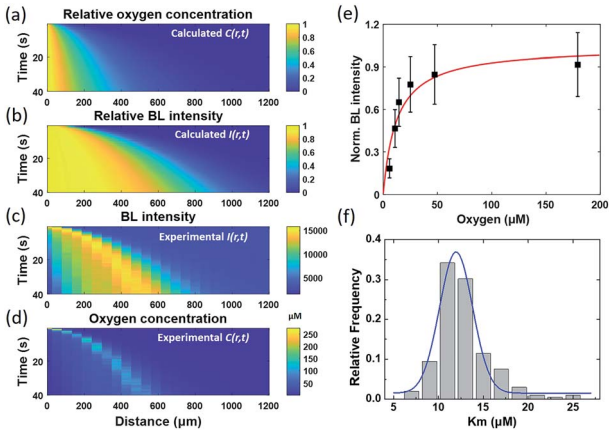

Fig. 4 Physical model allows for calculating the time-dependent distribution of (a) oxygen concentration $C(r, t)$, and (b) BL intensity $I(r, t)$, which is well consistent with the experimental results displayed in (c) and (d). (e) Dependence of BL intensity of a single BL bacterium on the oxygen concentration allows for determining the bacteria K_m by using the Michaelis–Menten equation. (f) The K_m histogram of 202 individual bacteria reveals an average value of 12 μM.

suggests that the BL intensity tends to saturate when the oxygen concentration is significantly larger than the K_m of luciferase.

$$I(r,t) = I_{max}\frac{C(r,t)}{C(r,t)+K_m} \quad (3)$$

Because the BL intensity is a direct and quantitative indicator of enzymatic reaction rate, the combination of both equations allows to calculate the relative BL intensity $I(r, t)$. In eqn (3), K_m in the physical model was experimentally determined by measuring the BL intensity of a single bacterium in solutions with different oxygen concentrations. Dissolved oxygen concentrations were regulated by adding different mass proportions of Na_2SO_3 (10%, 5%, 3%, 1%, 0.3%, 0.1%) to the culture medium for consuming oxygen, a popular method for culturing anaerobic bacteria. Then, the oxygen concentration of each solution was quantified by an oxygen reduction reaction with the rotating disk electrode method.[45] A perfusion system[46] was used to rapidly switch culture solution with different oxygen concentrations surrounding the bacteria of interest. Individual bacteria K_m values were obtained by fitting the oxygen concentration-dependent BL intensity with the Michaelis–Menten equation (Fig. 4e). The histogram of K_m values of 202 individual bacteria is shown in Fig. 4f, revealing an average K_m of 12 μM. This value was subsequently adopted in the physical model (eqn (3)) to calculate the relative BL intensity (Fig. 4b). The calculated result was nicely consistent with the results from the electrolysis experiment (Fig. 4c). Experimental oxygen concentration could be calculated based on the Michaelis–Menten equation, since the $I(r, t)$, I_{max}, and K_m were known. The result is shown in Fig. 4d. The total amount of oxygen was also estimated by integrating the chronoamperometric curve (i–t curve, Fig. S3†), which gave a value of 4.9×10^{-8} mol in an electrolysis time of 40 seconds (20^{th} to 60^{th} second in Fig. 2).

These results demonstrated an impressive sensitivity of bacteria bioluminescence for the detection of oxygen with a K_m of 12 μM. Because the bioluminescence of the bacterial luciferase system does not require the addition of external substrates, successful expression of the luciferase system (lux gene) has been achieved in prokaryotic cells,[27,47] mammal cells,[28,48] and plant cells.[49] A major challenge at the present stage is the relatively weak bioluminescence intensity. Wild type BL bacteria in our work exhibit sufficient BL intensity for individual bacteria imaging with an exposure time less than 1 second. If BL bacterial luciferase as a reporter could be expressed in different single cells with similar BL intensity, many dynamic processes in the biological system, such as tumor hypoxia and oxidative stress, could be monitored *in vivo* with improved exposure time and sensitivity, with implications for their biomedical and translational applications.

Spontaneous and stochastic oxygen wave

In the electrolysis experiments, an unexpected phenomenon came to our attention. When recording the baseline BL images of the bacterial monolayer without applying the potential and any disturbance, a spontaneous and stochastic BL wave was frequently observed. Movie S5† shows a typical BL wave video and the representative BL image snapshots are provided in Fig. 5a. It was observed that BL emission exhibited both significant spatial heterogeneity (on a scale of hundreds of microns) and temporal dynamics (on a scale of hundreds of seconds). Representative BL curves of three ROIs (marked by color squares) are shown in Fig. 5b, revealing significant intensity fluctuation by as large as 50%. The rapid increase and decrease of BL intensity also demonstrated excellent reversibility to report the oxygen concentration. The dynamic and heterogeneous BL intensity is also demonstrated in Fig. 5c, which displays the time-dependent intensity profile along a dashed line (shown in Fig. 5a) in a recording period of 2600

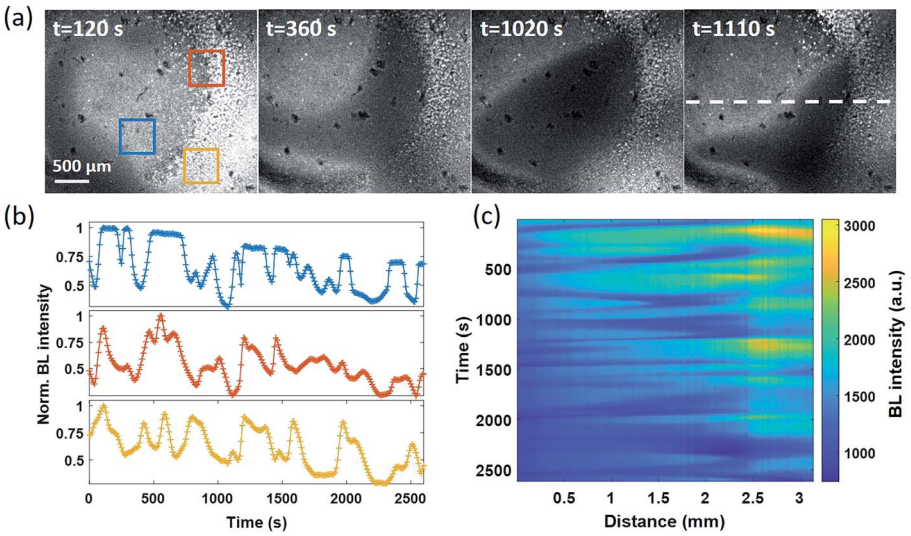

Fig. 5 (a) Representative BL images illustrate the spontaneous and stochastic features of BL waves (exposure time: 10 s). (b) The fluctuation of BL intensity as a function of time within three ROIs. (c) Time-dependent intensity profiles along a dashed line in (a).

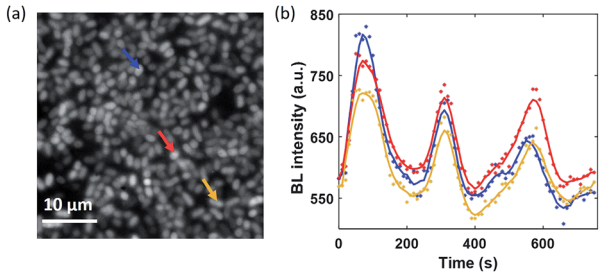

Fig. 6 (a) BL image of adhered bacteria within a ROI of 40 × 40 μm^2 (exposure time: 10 s). (b) Synchronized BL intensity curves of three adjacent individuals (mark with color arrows).

seconds. As demonstrated above, the BL intensity directly indicated the concentration distribution of oxygen molecules. The stochastic BL waves thus suggested that, although the solution in the chamber was undisturbed, the oxygen concentration at the liquid–substrate interface was inhomogeneous and underwent dynamic fluctuation.

Based on two experimental results, the BL wave was attributed to the micro-convection of liquid induced by evaporation, which resulted in the heterogeneous and dynamic distribution of oxygen. First, under some circumstances, the BL wave was accompanied by the directed movements of remaining individual suspending bacteria. Their trajectories were consistent with the BL wave, indicating the existence of micro-convection (Fig. S4†). Second, in order to examine the influence of local evaporation, a coverslip was placed on top of the chamber and was in contact with the culture medium to get rid of the gas–liquid interface (top interface) to minimize evaporation. It was found that the introduction of the glass coverslip largely inhibited the BL wave, in terms of not only the fluctuation ratio but also the time scale (Fig. S5†). However, even in the absence of solution evaporation, the heterogeneous distribution of oxygen was only inhibited, but not removed, indicating the remaining contributions from inevitable thermal fluctuations. To demonstrate the influence of thermal fluctuations, we introduced a local heating system to heat up the coverslip by taking the conductive indium tin oxide (ITO, 15–30 Ω) film as a resistor. When increasing the temperature of the coverslip underneath the solution, significant bioluminescent waves were observed as a result of the enhanced thermal fluctuations (Fig. S6†). The BL wave was further validated by single bacterial BL imaging as shown in Fig. 6 and Movie S6.† When plotting the BL intensity of individual bacteria as a function of time, all the curves were spontaneously fluctuating. This result validated that the fluctuating BL intensity was indeed due to the emission from individual bacteria as a result of heterogeneous distribution of oxygen, rather than the random movement and enrichment of suspending BL bacteria in the bulk solution.[50]

Because the distance between adjacent bacteria is only a few tens of microns in this case, it only takes less than 1 second for oxygen to diffuse 40 μm. As a result, temporal evolutions from different individuals were largely synchronized with a limited temporal resolution of 10 seconds.

Conclusions

In summary, by using an artificially generated oxygen wave induced by electrochemical oxidation of water as a model system, we have demonstrated the capability of the BL bacteria monolayer for visualizing the distribution of oxygen molecules in sensitive, real time and reversible manners. The *in situ* production of oxygen at the Pt surface resulted in oxygen diffusion towards the BL bacteria monolayer. The entire temporal–spatial feature was quantitatively explained by a physical model based on the diffusion equation and Michaelis–Menten equation. After the validation of methodology, BL imaging of the bacterial monolayer unexpectedly revealed a stochastic and spontaneous oxygen wave at the liquid–substrate interface in a well of a standard 96-well plate, which was attributed to the solution micro-convection induced by environmental factors including evaporation and intrinsic thermal fluctuation. Because the microtiter plate is routinely adopted in cell culture and bio-assays which relies on the homogeneous interactions with the molecules in the solution, these results shed new light to understand the apparent heterogeneity in relevant studies. The present study not only provides a powerful method to detect and visualize oxygen molecules by using BL bacteria, but also uncovers an unprecedented oxygen wave for studying the non-linear dynamics of reaction–diffusion systems, in addition to the famous calcium wave and Belousov–Zhabotinsky reactions.

Data availability

The datasets of this article have been uploaded as a part of the ESI.†

Author contributions

Y. Li carried out the experiments and analyzed the data. S. Wang and X. He helped with some experiments. S. Li provided methods for bacteria culture. T. Zheng helped optical setup improvement. Y. Chen and H. Cui read and commented on the manuscript. W. Wang conceived the project and wrote the paper.

Conflicts of interest

There are no conflicts to declare.

Acknowledgements

We thank the National Natural Science Foundation of China (Grants 21874070, 21925403 and 21876016), and the Excellent Research Program of Nanjing University (Grant ZYJH004) for financial support.

References

1 G. L. Semenza, *Science*, 2007, **318**, 62–64.

2 X. D. Wang and O. S. Wolfbeis, *Chem. Soc. Rev.*, 2014, **43**, 3666–3761.
3 E. H. Strickland, F. D. Ziegler and A. Anthony, *Nature*, 1961, **191**, 969–970.
4 F. Girard-sahun, V. Badets, P. Lefrancois, N. Sojic and F. Clement, *Anal. Chem.*, 2019, **91**, 8002–8007.
5 R. Zhu, S. M. Macfie and Z. Ding, *Langmuir*, 2008, **24**, 14261–14268.
6 X. Y. Dong, Y. Si, J. S. Yang, C. Zhang, S. Zang and T. Mak, *Nat. Commun.*, 2020, **11**, 3678.
7 L. Ding and X. D. Wang, *J. Am. Chem. Soc.*, 2020, **142**, 13558–13564.
8 E. Roussakis, Z. Li, A. J. Nichols and C. L. Evans, *Angew. Chem., Int. Ed.*, 2015, **54**, 8340–8362.
9 R. Xu, Y. Wang, X. Duan, K. Lu, D. Micheroni, A. Hu and W. Lin, *J. Am. Chem. Soc.*, 2016, **138**, 2158–2161.
10 X. Zhou, H. Liang, P. Jiang, K. Y. Zhang, S. Liu, T. Yang, Q. Zhao, L. Yang, W. Lv, Q. Yu and W. Huang, *Adv. Sci.*, 2016, **3**, 1500155.
11 C. Yin, H. Zhu, C. Xie, L. Zhang, P. Chen, Q. Fan, W. Huang and K. Pu, *Adv. Funct. Mater.*, 2017, **27**, 1700493.
12 Y. Li, J. Liu, Z. Wang, J. Jin, Y. Liu, C. Chen and Z. Tang, *Adv. Mater.*, 2020, **32**, 1907718.
13 S. Sakadzic, E. Roussakis, M. A. Yaseen, E. T. Mandeville, V. J. Srinivasan, K. Arai, S. Ruvinskaya, A. Devor, E. H. Lo, S. A. Vinogradov and D. A. Boas, *Nat. Methods*, 2010, **7**, 755–759.
14 H. Zhu, Q. Li, B. Shi, F. Ge, Y. Liu, Z. Mao, H. Zhu, S. Wang, G. Yu, F. Huang and P. J. Stang, *Angew. Chem., Int. Ed.*, 2020, **59**, 20208–20214.
15 C. Lu, C. Zhang, P. Wang, Y. Zhao, Y. Yang, Y. Wang, H. Yuan, S. Qu, X. Zhang, G. Song and K. Pu, *Chem*, 2020, **6**, 2314–2334.
16 J. Huang and K. Pu, *Angew. Chem., Int. Ed.*, 2020, **59**, 11717–11731.
17 K. Y. Zhang, P. Gao, G. Sun, T. Zhan, X. Li, S. Liu, Q. Zhao, K. K. W. Lo and W. Huang, *J. Am. Chem. Soc.*, 2018, **140**, 7827–7834.
18 Y. Zhou, W. Qin, C. Du, H. Gao and G. Liang, *Angew. Chem., Int. Ed.*, 2019, **58**, 12102–12106.
19 H. J. Knox, J. Hedhli, T. W. Kim, K. Khalili, L. W. Dobrucki and J. Chan, *Nat. Commun.*, 2017, **8**, 1794.
20 W. C. Geng, S. Jia, Z. Zheng, Z. Li, D. Ding and D. S. Guo, *Angew. Chem., Int. Ed.*, 2019, **58**, 2377–2381.
21 S. Takahashi, W. Piao, Y. Matsumura, T. Komatsu, T. Ueno, T. Terai, T. Kamachi, M. Kohno, T. Nagano and K. Hanaoka, *J. Am. Chem. Soc.*, 2012, **134**, 19588–19591.
22 S. Wilhelm and O. S. Wolfbeis, *Sens. Actuators, B*, 2011, **153**, 199–204.
23 S. H. D. Haddock, M. A. Moline and J. F. Case, *Annu. Rev. Mater. Sci.*, 2010, **2**, 443–493.
24 J. Li, L. Chen, L. Du and M. Li, *Chem. Soc. Rev.*, 2013, **42**, 662–676.
25 Y. Lin, Z. Ma, Z. Li, Y. Gao, X. Qin and Z. Zhang, *Anal. Chem.*, 2019, **91**, 14873–14878.
26 M. M. Calabretta, L. Montali, A. Lopreside, E. Michelini and A. Roda, *Bioluminescence Imaging*, ed. S. Ripps, Human, New York, 2020, pp. 3–14.
27 C. Gregor, K. C. Gwosch, S. J. Sahl and S. W. Hell, *Proc. Natl. Acad. Sci. U. S. A.*, 2018, **115**, 962–967.
28 C. Gregor, J. K. Pape, K. C. Gwosch, T. Gilat, S. J. Sahl and S. W. Hell, *Proc. Natl. Acad. Sci. U. S. A.*, 2019, **116**, 26491–26496.
29 Z. Frentz and J. Dworkin, *J. R. Soc., Interface*, 2020, **17**, 20200350.
30 J. J. Bourgois, F. E. Sluse, F. Baguet and J. Mallefet, *J. Bioenerg. Biomembr.*, 2001, **33**, 353–363.
31 F. J. Schindler, *Methods Enzymol.*, 1967, **10**, 629–634.
32 A. Roda, L. Cevenini, S. Borg, E. Michelini, M. M. Calabretta and D. Schüler, *Lab Chip*, 2013, **13**, 4881–4889.
33 M. Abbas, M. Adil, S. Ehtisham-ul-Haque, B. Munir, M. Yameen and A. Ghaffar, *Sci. Total Environ.*, 2018, **626**, 1295–1309.
34 L. Cevenini, M. M. Calabretta, G. Tarantino, E. Michelini and A. Roda, *Sens. Actuators, B*, 2016, **225**, 249–257.
35 D. Rosado, J. Usero and J. Morillo, *Chemosphere*, 2016, **153**, 10–17.
36 X. Qi, P. Liu, P. Liang, W. Hao, M. Li and X. Huang, *Biosens. Bioelectron.*, 2019, **142**, 111500.
37 H. Cong, Y. Liu, N. Ferré and W. Fang, *Chem.–Eur. J.*, 2014, **20**, 7979–7986.
38 S. Rozhok, Z. Fan, D. Nyamjav, C. Liu, C. A. Mirkin and R. C. Holz, *Langmuir*, 2006, **22**, 11251–11254.
39 Y. Liang, M. Li, T. Yuan, Y. Fang and W. Wei, *Chem. Sci.*, 2018, **9**, 3318–3323.
40 P. T. H. M. Verhallen, L. J. P. Oomen, A. J. J. M. v. d. Elsen, J. Kruger and J. M. H. Fortuin, *Chem. Eng. Sci.*, 1984, **39**, 1535–1541.
41 S. Scilipoti, K. Koren, N. Risgaard-Petersen, A. Schramm and L. P. Nielsen, *Sci. Adv.*, 2021, **7**, eabe1870.
42 K. H. Nealson, *Arch. Microbiol.*, 1977, **112**, 73–79.
43 M. B. Miller and B. L. Bassler, *Annu. Rev. Microbiol.*, 2001, **55**, 165–199.
44 K. Ngamchuea, S. Eloul, K. Tschulik and R. G. Compton, *J. Solid State Chem.*, 2014, **18**, 3251–3257.
45 M. Liu, Z. Zhao, X. Duan and Y. Huang, *Adv. Mater.*, 2019, **31**, 1802234.
46 W. Wei, Y. Yang, S. Wang, V. J. Nagaraj and N. Tao, *Nat. Chem.*, 2012, **4**, 846–853.
47 X. Tian, Y. Gao, S. Wang and T. Zhang, *Biosens. Bioelectron.*, 2021, **177**, 112919.
48 M. Conway, T. Xu, A. Kirkpatrick, S. Ripp, G. Sayler and D. Close, *BMC Biol.*, 2020, **18**, 79.
49 T. Mitiouchkina, A. S. Mishin, L. G. Somermeyer and N. M. Markina, *Nat. Biotechnol.*, 2020, **38**, 944–946.
50 R. SImkus, *Luminescence*, 2006, **21**, 77–80.